Honours Literature Review and Progress Report

Ryan White
Under the supervision of
Dr Benjamin Pope and Prof Peter Tuthill

July 21, 2024

1 Literature Review

1.1 Introduction

The understanding of massive stars in our Galaxy is foundational to our understanding of the Universe. Massive stars are born from the densest regions within clouds of molecular gas, and begin shaping their immediate environment and their galaxy from the outset. These stars evolve very quickly – on the order of a few to tens of millions of years – and produce an abundance of metals as they do so. As they live, massive stars eject material into the interstellar medium through their strong stellar winds and through episodic eruptions. As they die, massive stars enrich the chemical content of their galaxy through powerful supernova explosions. These two processes from massive stars, stellar mass loss and supernovae, are responsible for a significant proportion of the earliest metallic content in the Universe. In particular, the Wolf-Rayet (WR) stage of stellar evolution contributes a majority of this early carbon with which our Solar System was formed.

These Wolf-Rayet stars are the rare and extreme end-of-life phases of the most massive stars that have shed their hydrogen envelopes through binary interactions and the strongest known stellar winds. Within the Galaxy, only a few hundred of these WR stars have been observed. Given that they are some of the most intrinsically luminous stars, a larger population would be readily apparent if they were not so rare. Even though so few, these stars uniquely interact with the modern Milky Way and are understood to be the progenitors of the most energetic core-collapse supernovae, the Type Ic supernova. These supernovae have been associated with long gamma-ray bursts, whose energy output would be catastrophic to life on Earth were one to occur close enough and if oriented along our line-of-sight. Exactly how WR stars in the modern Universe may produce a gamma-ray burst is yet to be conclusively understood, but it is hypothesised that certain binary interactions may impart enough angular momentum onto the progenitor WR star for this to take place. Since a majority of massive stars are formed in binary or multiple systems, WR binaries are of particular interest.

Without having direct observations of a Wolf-Rayet supernova taking place, the current population of WR stars must be closely studied to better our understanding of the final moments of massive stars. Of particular interest are the colliding wind binaries (CWBs) that host WR stars. When a WR star and a sufficiently massive companion are in a close binary, we often observe a so called wind collision region (WCR) where carbon-rich dust is nucleated at the collision interface between the stellar components' winds. This dust is bright in the infrared and traces the orbital motion of the binary itself, forming an intricate spiral structure as the dust plume expands away from the system. This process is like a sprinkler, throwing out material along a narrow cone while rotating with the orbital motion of the binary stars. When the orbital motion is inclined to be almost entirely in the plane of the sky, the dust nebula forms an Archimedean spiral, or a so called 'pinwheel nebula'. At different inclinations, the produced spiral nebulae are geometrically unique and can often resemble bubbles. This spiral structure encodes precisely the underlying physics of CWBs and by extension WRs and their companions.

Apep, a WR+WR system which is perhaps one-of-a-kind in the Galaxy, stands out as one of the most interesting examples in an already unique class of star system. It is surprising to find a binary system with both stars in this short-lived phase of stellar evolution, and the evolution mechanism for this is an unsolved problem. Apep's orbit is too compact and too far away for us to easily resolve orbital motion, an effort which is further complicated by the intricate colliding wind nebula enshrouding the system. This nebula, however, encodes much of the orbital and wind physics of the two WR stars at its center. Therefore, modelling the spectacular nebula of Apep will help us understand the most likely gamma-ray burst progenitor in the Galaxy.

In this Section we begin by reviewing the stellar evolution of massive stars to the Wolf-Rayet stage. We go on to describe the properties of Wolf-Rayet stars and their role in the evolution of galaxies (chemically and otherwise). Since massive stars are often born and evolve in binary systems, we discuss the prevalence of WR binary systems and their unique observables. Naturally this leads to the presence of colliding wind binaries, where

we overview their impact on the Galaxy, the methods done to model these and the gaps in these methods (in particular the geometric modelling).

1.2 Massive Stellar Evolution and Wolf-Rayet Stars

Massive stars, those of order 10 to $100M_{\odot}$, like other stars form in giant molecular clouds (de Wit et al., 2005; Tan et al., 2014). The initial masses of stars formed within these molecular clouds follow an initial mass function (IMF) such that low mass stars are much more often formed than high mass stars (Miller & Scalo, 1979; Kroupa, 2001). Even though formed in fewer numbers, the exponentially higher radiation inherent with massive stars means that they are the dominant force in shaping their parent molecular clouds once star formation begins (Motte et al., 2018), ionising gas in so-called HII regions. As a molecular cloud contracts under its self-gravity, the cloud fragments and forms stars along filamentary structure (Hoyle, 1953; Chira et al., 2018; Hacar et al., 2023). The closest forming protostars along these filaments interact gravitationally and, supported by complex hydrodynamical processes, often form binary or multiple systems. As massive stars naturally form in regions of higher density (and in addition to their correspondingly higher gravitational influence), there is a strong preference for binarity/multiplicity in massive star systems and with stars of comparably high mass (Sana & Evans, 2011; Sana, 2017; Offner et al., 2023). The impact that binary WR stellar evolution has on supernovae is discussed in Section 1.3, and the multiplicity of binary WR systems in Section 1.4.

Once a molecular gas core has contracted into a massive protostar, the protostellar core quickly becomes convective and hot enough to fuse hydrogen, helium and carbon (Carroll & Ostlie, 2017; Motte et al., 2018); the protostar enters the main-sequence as an O or B type star. It is in this main-sequence phase that all stars spend the majority of their lives, predominately burning hydrogen into helium and heavier elements via the CNO cycle (Maeder, 1983; Woosley et al., 2002; Carroll & Ostlie, 2017). After several million years the hydrogen in the convective core is exhausted and the star leaves the main sequence, forming heavier elements via the triple-α process (Salpeter, 1952; Woosley et al., 2002; Carroll & Ostlie, 2017).

During a phase of core/shell helium or carbon-oxygen burning, massive stars usually evolve into supergiant stars. Depending on the initial mass of the star, this could mean a red or blue supergiant (RSG and BSG respectively), or a luminous blue variable (LBV) star in the latter case (Groh et al., 2013). Whether through one of or a combination of mass loss through stellar winds and/or binary mass transfer, the highest mass ($\gtrsim 20M_{\odot}$) stars shed their outer hydrogen envelopes leaving an exposed helium star or Wolf-Rayet star (Paczyński, 1967; Conti, 1975; Crowther, 2007). The exact progression of envelope/mass loss is a topic of active research, and depends very sensitively on the mass, metallicity and rotation of the star among other variables (Meynet et al., 2011; Sander & Vink, 2020; Josiek et al., 2024); the most massive stars ($> 25M_{\odot}$) may skip the supergiant phase altogether and evolve off the main-sequence directly into a WR star (Crowther, 2007; Groh et al., 2013).

Wolf-Rayet stars are characterised by extremely strong, dense stellar winds driven by emission lines of helium, carbon, nitrogen, and/or oxygen (Wolf & Rayet, 1867; Hamann et al., 2006; Crowther, 2007). Despite the hydrogen envelope shedding and high mass loss rates, WRs remain very massive at $\gtrsim 10M_{\odot}$, depending on their spectral type. Within the Wolf-Rayet classification, there are 3 main subclassifications: the WN type (owing to strong He and N lines), the WC type (owing to an absence of N and prominence of C), and the WO type (an absence of N and strong presence of O) (Gamow, 1943; Crowther, 2007). Within each of these subclassifications there exist subtypes that describe the relative strength of individual emission lines (WN2-11, WC4-9, and WO1-4) and hence more specific chemical and physical properties of the stars. The relationship between the different classes of WR stars has long been understood to in a progression from one type to another (depending on the initial mass of the star Conti, 1975; Abbott & Conti, 1987), but this has been recently challenged (McClelland & Eldridge, 2016) indicating that even the fundamental properties of these stars are still a topic of active research.

Despite unknowns in their evolutionary progression, much about the phenomenology of Wolf-Rayet stars is well known and observed. Of particular note is their uniquely strong stellar wind. There are multiple observational probes that suggest these winds, both intrinsic (e.g. line broadening in spectra) and extrinsic (in the interaction with the WR surrounds).

Perhaps the most robust indicator of a WRs wind velocity is in its spectrum. Observing individual emission lines in the spectrum of a star often shows a P Cygni profile, where the line is broadened by the expansion of the luminous wind in both radial directions (simultaneous red and blue shifting), and absorption of star light from wind material directly along the intermediate line of sight to the star imposes a strongly blueshifted absorption line. By analysing the shape of this line profile, highly precise wind speeds are obtained (Willis, 1982; Crowther, 2007; Callingham et al., 2020; Williams et al., 2021). Zavala et al. (2022) also showed that by taking several spectra at different regions of a WR nebula, a three dimensional geometric model of the nebula can be produced that encodes information not only about the wind speed, but direction too.

Interactions of the Wolf-Rayet wind with the sur-

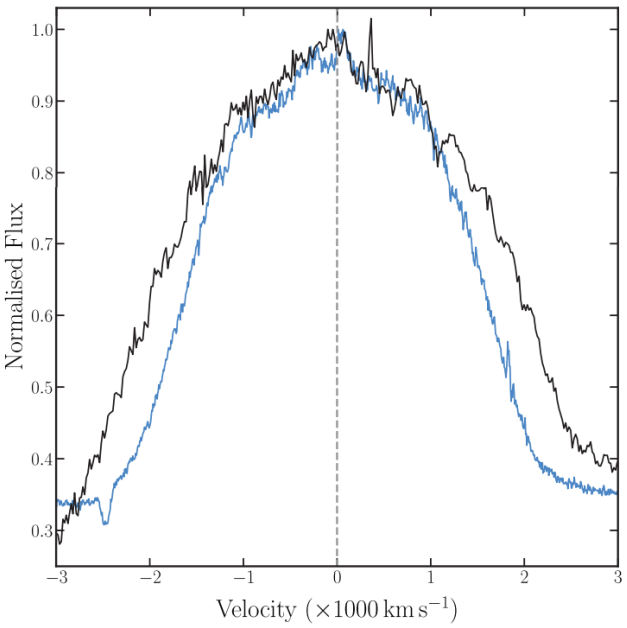

Figure. 1 The spectrum of the WR+WR system Apep shows some lines with a P Cygni profile (here the HeII 1012nm line in blue) and some without (the black CIII 971nm line) – an indication of two stars with different wind speeds (Callingham et al., 2020). Already converted from wavelength into radial velocity, we see the characteristic absorption dip at about −2500km/s.

rounding enviornment strongly constrain their wind physics. Wind-collision regions, and ablation and/or ejecta in nebulae/molecular clouds surrounding the stars are the main observational probes of interaction. We defer discussion of the former to Section 1.5. Over the course of the WR phase, the stellar winds of the stars often form bright nebulae (see: NGC 2359, NGC 6888, Hf 39); studying the multi-epoch expansion of these nebulae reveals the distances to these systems if the wind velocity is well constrained (or vice versa). One such case where nebula expansion has been observed is in the wind nebula M1-67 around WR 124 (Marchenko et al., 2010) which allowed for an independent distance estimate to the system; this has also been done with the WR nebula BD+30°3639 (Schönberner et al., 2018). As a secondary direct imaging probe of WR winds, WR stars have been observed forming cavities in the molecular material of their natal environment via ablation from their stellar winds (Baug et al., 2019, see also Dale et al., 2013 for simulations of this). This same process has been seen forming shocks when the wind interacts with the surrounding gas, often triggering more star formation (Cichowolski et al., 2015).

In addition to high wind speeds, Wolf-Rayet stellar winds have some of the highest mass loss rates of any stellar type (comparable only to LBVs and RSGs). It's understood that this mass loss is primarily driven by the radiation pressure of metallic emission lines (Castor et al., 1975; Crowther, 2007), the WR stars themselves being near the Eddington limit (Gräfener & Hamann, 2008; Gräfener et al., 2011). Mass loss rates for WR stars are typically on the order of $10^{-5} M_{\odot}$ yr^{-1} (Barlow et al., 1981; Crowther, 2007), and so this coupled with the high wind velocity means that WR winds have exceptionally high momentum.

Much of the mass within the stellar winds is inhomogeneous, being clumpy and nucleating into dust at sufficient distance. Although WR stars have mostly steady winds, there is an observed small-scale stochasticity in the winds that manifests as multi-epoch line variation (Michaux et al., 2014; Chené et al., 2020); hence, the WR stellar wind can be chemically inhomogeneous. On a related note, circumstellar dust is produced around many WR stars, especially those of WC subclassification (Allen et al., 1972; Gehrz & Hackwell, 1974; Lau et al., 2021). How delicate dust molecules are formed around WR stars – some of the hottest and most ionizing astrophysical environments in existence – is still a topic of active research. The clumpy wind is one proposed avenue for dust formation, where the high opacity and density within clumps provides a sort of shielding from the environment where molecules can form (Cherchneff et al., 2000). Another notable avenue is in the wind collision region of WR binaries, where turbulence in the enriched wind shock cone produces dust very efficiently (Soulain et al., 2023). This will be discussed more in Section 1.5.

1.3 Wolf-Rayet Stars as Supernova Progenitors

Wolf-Rayet stars are convincing candidates for Type Ib/Ic supernovae (SNe Ibc) progenitors: WRs are massive pre-supernova stars that lack hydrogen spectra, as do SNe Ibc (Filippenko, 1997; Crowther, 2007; McClelland & Eldridge, 2016). There is some discussion of an alternate SNe Ibc channel in Smartt (2009) where a lower mass star may lose its hydrogen envelope via binary interactions prior to undergoing supernova (not dissimilar to one of the proposed channels of WR formation). The consensus is that at least some combination of the WR progenitor model and this alternate scenario explain the observed population of SNe Ibc (see: Eldridge et al., 2013; Pellegrino et al., 2022; Karamehmetoglu et al., 2023).

Despite their intuitive connection, no WR stars have been definitively shown to be SNe Ib/c progenitors with pre-supernova imaging of galaxies. Kilpatrick et al. (2021) identified the likely progenitor of Type Ib supernova SN2019yvr in Hubble Space Telescope imagery taken 2.6yr prior to explosion. They found that neither a clear-cut WR nor a lower mass binary can adequately describe the SN progenitor, indicating that perhaps a sudden change in the observables of SNe Ibc progenitors take place just prior to explosion, e.g. extreme mass loss.

The lack of attribution could also plausibly be ascribed at least in part to the reduced detectability of WR stars at extragalactic distance (Pledger et al., 2021).

Where some connection has been made is between Type Ic supernovae and gamma-ray bursts (GRBs). Gamma-ray bursts are a class of energetic transient whose duration distinctly fall into two categories of 'short' and 'long', with several sources appearing isotropically on the sky each day (Woosley & Bloom, 2006). Short GRBs, of order $\lesssim$ 2s, are understood to be the result of kilonovae, the breakup of degenerate neutron stars during gravitational wave induced binary inspiral (Berger, 2014). Long GRBs (LGRBs), of order $\gtrsim$ 2s, are understood to be the result of the relativistic jets produced in the core-collapse of highly rotating massive stars (Woosley & Heger, 2006). One might then expect that LGRBs follow largely similar progenitor scenarios to SNe Ic. In fact, several SNe Ic-BL events, SNe Ic with especially broad spectal lines indicative of relativistic ejecta, have been definitively associated with LGRBs (Galama et al., 1998; Ashall et al., 2019). Interestingly, not all of these SNe Ic-BL have been associated with LGRBs, though, indicating that the jets are highly collimated (and hence their visibility being very direction dependent) or there remains a significant gap in understanding (Siebert et al., 2024).

The consensus on the LGRB progenitor mechanism lies within the collapsar model where at the time of supernova, the innermost core collapses into a black hole (BH). The surrounding core, having a high enough angular momentum to form a disc, produces polar jets as a result of angular momentum loss as matter accretes onto the natal BH (Woosley, 1993; Dean & Fernández, 2024). For a star to do this, it must have extremely high angular momentum. This should be the case for stars that have been efficiently mixed during their life times (Woosley & Heger, 2006), and hence stars that are effectively free of hydrogen at supernova as a result; thus it is not a requirement that there is no hydrogen at the GRB (and hence a Type I SNe vs a Type II), but rather a consequence of the evolutionary process that gives rise to GRBs. Because of this, helium and metal rich stars emerge as the leading candidate progenitors for SNe Ic/-BL. There is a significant body of simulations linking WR to SNe Ic and GRBs through the collapsar model (McClelland & Eldridge, 2016; Aguilera-Dena et al., 2018), especially those with high rotation at preferentially low metallicity (Detmers et al., 2008).

1.3.1 Metallicity in Different Epochs

Modern Wolf-Rayet stars are synonymous with metallic line-driven winds. These winds, along with magnetic effects, are known to be efficient at dissipating angular momentum from hot stars (Woosley & Heger, 2006; Ud-Doula et al., 2009). This, in conjunction with the more efficient mass-loss at high metallicity (Vink & de Koter, 2005; Gräfener & Hamann, 2008), means that we generally expect high metallicity WRs to be slower rotators. There is a strong connection between rotation speed of a progenitor star to its LGRB status (and also between the spin of the collapsar BH to the GRB jet collimation; Hurtado et al., 2024), and so the logical conclusion is that we should expect fewer or no LGRBs in evolved galaxies with high metal content.

Indeed, there is strong indication from stellar models that low-metallicity massive stars should be rapidly rotating (Chiappini et al., 2006; Vink & Harries, 2017). This motivates searches for LGRB progenitors in dwarf and/or satellite galaxies where the metal content can be as low as orders of magnitude below Solar metallicity (Tolstoy et al., 2009). There has been some plausible, if inconclusive, evidence of rapid rotating WRs in the Large Magellanic Cloud (Shenar et al., 2014; Vink & Harries, 2017), lending credence to this idea. Therefore we expect that LGRBs are efficiently produced in the early universe or in dwarf galaxies with less enriched chemical content.

One proposed channel for fast spinning massive stars, and hence LGRB events, within chemically evolved galaxies like the Milky Way is in the tidal spin up from a closely orbiting binary companion. Early studies suggest that this mechanism is improbable at solar metallicity and marginally more likely at low metallicity (Detmers et al., 2008). More recently, population synthesis studies have shown this to be an efficient mechanism to quickly rotating evolved stars (Chrimes et al., 2020; Bavera et al., 2022), although only in very closely orbiting binaries.

1.4 Binary and Multiple Systems

There is an apparent link in models between the rotation rate of massive stars and their binarity, and there is clear evidence that massive stars often form in binary or multiple systems within the Galaxy (Offner et al., 2023). This begs the question of how Wolf-Rayet stars fit within the picture of binary/multiple systems, and what this means for their evolution and observation.

Massive O stars on the main sequence are most commonly formed within binary or multiple systems, where their companions are usually massive OB stars too (Shara et al., 2022; Offner et al., 2023). Naturally, as the primary stars in these systems evolve off the main sequence into BSG or WR stars, the tend to keep their companions. Eventually, the primary star is expected to undergo a supernova in which case the secondary may be ejected as a 'runaway star' with very high velocity (of order orbital velocity at the time of supernova, up to $\sim$ 120km/s; Eldridge et al., 2011). This means that although surveys may identify single O/B/WR stars, they may have still been formed as a binary system (Schootemeijer et al., 2024). Regardless, the Galactic WR binarity fraction is reported as $\sim$ 40% (van der Hucht, 2001; De Marco & Izzard, 2017) and surveys of the lower metallicity Large and Small Magellanic Clouds (LMC

and SMC, $Z \sim 0.5Z_\odot$ and $Z \sim 0.2Z_\odot$ respectively) suggest similar values indicating that binarity is not a function of metallicity or redshift (Foellmi et al., 2003; Shenar et al., 2020; Schootemeijer et al., 2024)

Wolf-Rayet binaries do not fall into any single categorical box. Companions have been found in both very close and very wide orbits, and interestingly there appears to be at least some orbital period preference versus WR type: WN stars are more commonly found in close binaries, and WC in wide binaries (Dsilva et al., 2020, 2022, 2023). Also, while WR companions are usually similarly (or more) massive O stars there are several confirmed and tentative detections of unusual companion types. Of particular note is the possible detection of a low mass F type main sequence companion to WR 113, making the system a triple with its known WC8 + O8 components (Shara et al., 2022). In the same study the authors propose a detection of a wide orbit WN3-4 companion to the WN7 star WR 120, making one of the only known WR+WR systems known. WR 48a has been proposed as a candidate WC8+WN8 system on the basis of its spectra (Zhekov et al., 2014). Apep (WR 70-16) has been confirmed as a WC8+WN4-6 binary due to the clear wind speed discrepancy in its spectrum (Callingham et al., 2020, Figure 1) together with a superposition of spectral lines characteristic of specifically those two classes of WR star. Both of these WC+WR systems are in long-period orbits (> 10 years), and a confirmed WN6+WN6 system, WR 20a, has been observed with a very short few day orbit (Bonanos et al., 2004; Rauw et al., 2005).

How two Wolf-Rayet stars evolve in the same system at the same time is, like Wolf-Rayet evolution in general, still an open question. Early studies even questioned the observability of these systems (Vrancken et al., 1991), although technique and instrumentation development has provided clear success in detection of WR binaries. With a lack of population synthesis studies showing a clear WR+WR formation channel, the best indication may lie in the study of less evolved massive stars (e.g. in the WN6h+O3/WN7 system R145; Shenar et al., 2017)

1.5 Colliding Wind Binaries

Given that Wolf-Rayet stars are known by their intense winds and high binarity fraction, it naturally arises that we should expect some interaction at the collision interface between the winds of the WR star and its massive companion (Cherepashchuk, 1976; Prilutskii & Usov, 1976). Indeed, there is a modest population of WR+O/B/WR binaries whose dense wind collide to produce dust nebulae that expand away from the system. We show a diversity of such systems in Figure 2, showing that even the same physics can produce vastly different spiral structure.

All dust producing colliding wind binaries observed to date are composed of a cool, late type WC star whose wind contains the key ingredients for dust. In the wind collision region, these ingredients are forced to combine and are shielded from the ionizing radiation in the turbulent conical shock boundary (Hendrix et al., 2016). The result is a very bright dust nebula in the infrared whose geometry and periodicity reveal otherwise hidden orbital parameters of the system.

Some of the first indication of dust production in a colliding wind binary was in the periodic infrared brightening of WR 140 (Williams et al., 1978, 1987), where the wind collision region and subsequent turbulent shock provides an ample environment for dust production (Williams et al., 1990; Usov, 1991). The spiral structure in these nebulae arise from the shock cone produced at the collision interface wrapping around from the orbital motion of the stars.

With this in mind, we see relatively clean Archimedean spirals produced in binary systems where the components have roughly circular orbits (see WR 98a and WR 104, Figure 2), so called 'pinwheel nebulae' due to their regularity. Systems with elliptical binary orbits show less predictable repeatability, often associated with orbital modulation in the dust production that manifests as a 'turn on' and 'turn off' in the spiral (see Apep, WR 140 in Figure 2). This, coupled with the range of inclinations that these systems can have relative to our line of sight, means that no two colliding wind nebulae appear the same despite a relatively consistent formation mechanism.

1.5.1 A Short Catalogue of Key CWBs

We present here some of the most unique and significant (historically or otherwise) Wolf-Rayet colliding wind binaries for ease of reference. These WR binaries in particular stand out as some of the most vital systems in our understanding of massive stellar physics, both in the past and into the future. By studying them we may peer into the process by which the first carbon in the Universe was produced, and how the environment around these stars shapes (often literally) their contribution to the evolution of our Galaxy.

Apep One of the only confirmed WR+WR systems, and certainly the only known to have a WC with a dust nebula (Callingham et al., 2020), Apep was long known as a bright X-ray and radio source and potentially the brightest of all the CWBs. It was recently observed with the VLT which showed its spiral dust nebula structure (Callingham et al., 2019; Han et al., 2020). Likely a triple system, there is an O8 star very close to the north of the WR+WR inner binary with some indication of association. This is one of the primary motivators of my Thesis, and is discussed in Section 2 of this report.

WR 48a At present, this is the only other candidate WC+WN CWB – specifically WC8+WN8h

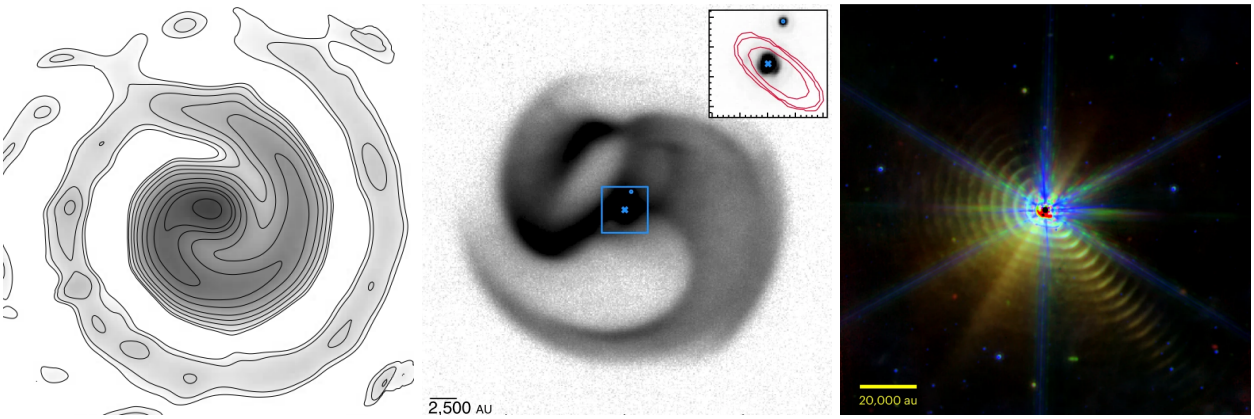

Figure. 2 The last ∼ 20 years has seen much progress in imaging the dust nebula colliding wind binaries. *Left:* The first imaged CWB, WR 104 (Tuthill et al., 2008), done so with reconstructed images of interferometric data. *Center:* Perhaps one of the only WC+WN systems in the Galaxy, Apep (Callingham et al., 2019) taken with the VISIR instrument on the Very Large Telescope. *Right:* The first CWB directly imaged with the James Webb Space Telescope, WR 140 (Lau et al., 2022), shows several concentric shells of dust production.

(Zhekov et al., 2014) – found to be in an orbit with eccentricity $e \sim 0.6$ (Williams et al., 2012). This was one of the first objects to be identified as a colliding wind binary, and was first directly imaged in Marchenko & Moffat (2007). Like Apep, WR 48a has a relatively long orbital period of ∼ 32 years and displays variable dust production throughout its orbit (although there is no evidence of a complete dust 'turn off' in WR 48a as in Apep).

WR 98a One of the first colliding wind nebulae to be directly imaged, this system showed the first imaging evidence of inclination effects in a pinwheel nebula (Monnier et al., 1999), in contrast to the Archimedean spiral of WR 104.

WR 104 As the first colliding wind binary to be directly imaged, WR 104 emerged as the prototype 'pinwheel nebula' from the clear evidence of orbital motion in its dust plume (Tuthill et al., 1999). This system has been the subject of intense study, particularly in hydrodynamical simulations and the application of pinwheel structure to other CWB nebulae. Like WR 98a, WR 104 is a reasonably short period WC+O binary ($\lesssim$ 2 years) in a very circular orbit (Tuthill et al., 2008). Recently, a B star distant from the WC+O binary was considered as being associated with the system (Wallace et al., 2002; Soulain et al., 2018), potentially making WR 104 one of the very few known WR triple systems.

WR 112 First imaged in 2002, the colliding wind nebula of WR 112 was the first to visibly reveal concentric shells of dust formation (Marchenko et al., 2002) from its inner WC8+O binary (Lau et al., 2020). Like the other consistent dust producers listed here (WR 98a, 104), WR 112 has a well constrained eccentricity close to 0 as is evident from its regular concentric shell structure. Notably, the pinwheel nebula structure was incorrectly applied to WR 112's dust nebula twice, yielding far-off estimates of the nebula expansion speed and the binary eccentricity and inclination (Marchenko et al., 2002; Lau et al., 2017).

WR 140 The 'prototype' colliding wind binary, composed of WC8+O5 stars on a very high eccentricity ($e \sim 0.89$) orbit of about 7.9 years (Williams et al., 2009; Monnier et al., 2011). This was the first system to be inextricably linked as a colliding wind binary, in no small part due to its modulation of dust production: the dust seen in Figure 2 (right-side) is produced only in a narrow time frame as the stars approach and leave periastron (Lau et al., 2022; Han et al., 2022). This is perhaps the most well studied of all CWBs across all wavelengths and imaging techniques.

WR 147 An apparent triple system composed of a WN8, a close unseen companion, and a distant OB star (Rodríguez et al., 2020). This is the first ever system to have an observed pinwheel from the inner binary not in the infrared but in the radio. Not only this, but there is a well resolved bow-shock distinct from the pinwheel where the winds collide with the tertiary component. This aligns with previous X-ray observations that resolved the system as a double X-ray source: one at the inner binary and another at the WCR of the inner binary relative to the outer companion (Zhekov & Park, 2010a,b).

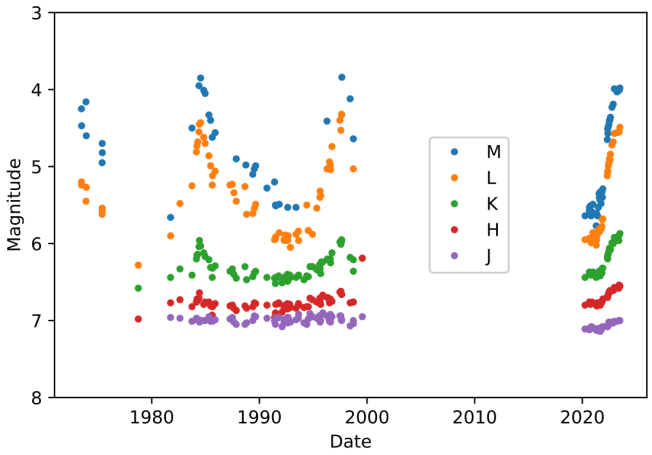

Figure. 3 The long-term infrared light curve of WR 137 shows episodic dust production in the periodic peaks. Shown here is the photometry across different infrared bands (descending band central wavelength in the legend), where the deeper infrared shows brighter total emission as a result of dust production. As the stars approach periastron every $\sim$ 13 years, dust production turns on and eventually turns off after the stars are again sufficiently far apart. Figure from Peatt et al. (2023).

1.5.2 Photometry and Spectra

The first indication of and the longest used tools for analysing colliding wind binaries has been direct photometric and spectral observation. Systems with episodic dust production, especially those with non-negligible eccentricity, are clear photometrically due to their periodic peaks in infrared brightness. This is especially notable in relatively short period systems such as WR 140 ($P \sim 7.9$ years) and WR 48a ($P \sim 32$ years) where mostly complete light curves have been made since the discovery of CWBs (Williams et al., 1987, 2012; Peatt et al., 2023; Richardson et al., 2024). This is potentially the 'cheapest' way to discover new CWBs due to the nature of photometric observation; the exact target does not need to be observed for long exposures, only snapshots at many periods in time (perhaps even when only in the field of another target). Light curve analysis is still being used even recently to discover episodic dust producers who likely lie in CWBs (Williams, 2019). Not only their in their discovery, but the properties of CWBs can be discerned from the dust production light curve profile and so this is a useful tool in monitoring known systems.

An earlier clue for dust formation in Wolf-Rayet binaries was in their spectra. Dust produced in these systems is relatively cool (of the order $\lesssim$ 1000K), and so has peak blackbody emission in the infrared (van der Hucht et al., 1996, for dust peaks around 10-15μm in WR 48a, 98a, 104, 112, and 118). Due to the abundance of dust produced absorbing higher energy light and re-emitting it in the infrared, these dust peaks have an infrared luminosity far in excess of the system stars (Gehrz & Hackwell, 1974; Williams et al., 1978). Analysing the spectra of these systems remains a key tool in understanding their wind composition, and also their orbits (for example the spectral decomposition of WR stars in Callingham et al., 2020).

A recent spectral analysis of a dust shell of WR 140 suggested that there exists not just one infrared peak of carbon dust emission, but two: one dust species of $T \sim$ 1000K and grain size $\sim$ 1nm, and another of $T \sim$ 500K and size 30-50nm (Lau et al., 2023). The analysis further showed that the ratio of these species varies in the shell number (or rather the age of the dust), and so the dust properties of any CWB are constantly evolving not only in production but in composition too.

Another promising avenue to study Wolf-Rayet stars through their spectra is in the method of spectropolarimetry. This method provides an unambiguous probe into the asphericity (or more generally anisotropy) of a stellar wind via any discrepant polarisation between continuum and line emission (Harries et al., 2000; Vink et al., 2011, see the later for a succinct description of the method). This method has been successful in identifying wind asphericity and rapid rotation in several classes of stars, including WRs, and even in the WC+O CWB WR 137 (Harries et al., 2000; Lefèvre et al., 2005). It is currently not unambiguously clear, though, if this method is valid as a signal of stellar rotation in the environment of a WCR.

Colliding wind binaries are strong X-ray sources, and were first hypothesised in Cherepashchuk (1976); Prilutskii & Usov (1976). Since the association of CWBs with X-ray sources, the theory modelling their properties has matured and accurately represents observations (Rauw & Nazé, 2016, for a review). Modern models reproduce X-ray spectra exceedingly well, providing insight into the mass loss rates and windspeed but also the homogeneity of the wind and its cooling physics (Zhekov, 2021; Zhekov et al., 2022). The X-ray flux of eccentric CWBs is variable as the properties at the WCR change over the course of the orbit, allowing us to constrain orbital and dust production properties; the phase of the flux peaks has been found to be wavelength dependent as the most efficient cooling mechanism at the WCR changes between radiative and adiabatic with orbital phase (Gosset & Nazé, 2016; Rauw & Nazé, 2016; Mackey et al., 2023). This kind of variation within the light curve is in conjunction with the usual eccentricity effects, as well as a WCR column density constraint on the orbital inclination in the X-ray (see Section 5.3 of Gosset & Nazé, 2016).

Colliding wind binaries are also luminous in the radio, observed as far back as 1976 (Seaquist, 1976; De Becker & Raucq, 2013). The wind collision region in these systems acts as a particle accelerator, efficiently producing relativistic electrons that then emit radiowaves via synchrotron radiation (Eichler & Usov, 1993; Bloot et al.,

2022). As such, radio observations of CWBs offer information of the WCR directly, even so far as identifying the WCR itself with interferometric imaging (see Dougherty et al., 2005; Marcote et al., 2021). Since radio observations constrain the WCR so well, any discrepancies between wind models and data (e.g. momentum ratios, mass loss rates, etc) are immediately apparent. Recently, radio observations of Apep were used to constrain its wind asphericity, where Bloot et al. (2022) found a preference for an anisotropic wind, with the WC star at an inclination angle of $(22 \pm 6)^\circ$ to the orbital plane. These studies are integral to our understanding of WRs as rapid rotators, as is to be expected from an aspherical wind, and their role as LGRB progenitors.

1.5.3 Direct Imaging

Although the dust nebulae produced by colliding wind binaries are orders of magnitude larger than the solar system (see the scales in Figure 2), their Galactic distance of $\gtrsim$ 1kpc requires that high angular resolution observations are needed to resolve structure. This, coupled with the fact that the resolved dust nebulae are luminous only in the infrared, means that direct imaging of these nebulae is a recent development in astronomy coevolving with high angular resolution infrared astronomy. Directly imaging these nebulae is an essential effort as we can more precisely constrain many of the orbital parameters compared to other methods, and learn about some parameters that are not constrained by, or possible with, spectral or photometric analyses (see Section 1.5.5). The first imaging of these systems was done with interferometric imaging on Keck for WR 104 and WR 98a (Tuthill et al., 1999; Monnier et al., 1999). The past 20 years have seen an explosion of ground-based high angular resolution infrared astronomy, where direct images of colliding wind nebulae has become almost routine on large telescopes (Marchenko et al., 2002; Marchenko & Moffat, 2007; Tuthill et al., 2008; Callingham et al., 2019, for WR 112, 48a, 104/98a and Apep respectively), even for very distant systems near the galactic center (Tuthill et al., 2006).

Very recently, the James Webb Space Telescope (JWST) has begun observing colliding wind binaries. JWST has made visible dust emission that would otherwise be hindered by atmospheric effects. This has allowed observation of cool dust at a greater distance from the central CWB engine, and hence the simultaneous observation of several orbital periods worth of dust shells in the nebulae (Lau et al., 2022).

1.5.4 Hydrodynamical Simulations

Perhaps the most rigorous, if also computationally intensive, treatment of colliding wind binaries is with hydrodynamical simulations. Therein the complicated interactions of gas and dust in the environment around the WR binary can be simulated, offering insight into dust production and the chemical content of CWB nebulae.

These simulations are essential in predicting the geometric dust production around the shock, as well as comparing the state of theory with observations. Notably, hydrodynamical simulations were used to suggest that dust production is more efficient around the trailing edge of the shock than the leading edge (with respect to the orbital motion of the stars Lamberts et al., 2012; Hendrix et al., 2016; Soulain et al., 2023). This is observationally confirmed by the 'azimuthal variation' in dust production around the shock cone of WR 140 in particular (Williams et al., 2009; Han et al., 2022).

Hydrodynamical simulations have helped show just how sensitive dust production is to system parameters, explaining in large part the diversity of colliding wind nebulae. Not only has mass loss rate, wind velocity and wind chemical composition been shown to alter the shock properties (Eatson et al., 2022a; Soulain et al., 2023), but even the speed of orbital motion has been suggested as a key factor in the turn on vs turn off true anomaly in eccentric systems, such as WR140 (Eatson et al., 2022b). Further, these simulations are consistently used in the reproduction of non-thermal (primarily X-ray and radio) observations (Pittard & Dougherty, 2006; Mackey et al., 2023).

1.5.5 A Geometric Model

In parallel with the maturation of hydrodynamical simulations, various simple geometric models were developed to reproduce key features of colliding wind nebulae. These geometric models allow for far simpler parameter estimation of CWBs and at much faster compute time compared with hydrodynamical simulations. Archimedean spirals have been used since the first direct images of these dust nebulae (Tuthill et al., 1999), although this does not account for the volumetric geometry of the dust plume and is valid only for a narrow range of binary inclinations. Since then, a more physically motivated geometric model has been developed which reproduces the volumetric structure of the expanding plume. The model approximates the wind collision region as a ring surrounding the shock cone which is initialised with the radial wind velocity. When populating a high number of rings over the orbital period, the result is a discretised expanding plume structure that faithfully emulates the true geometry of the dust nebula when interpolated. This family of geometric models was first shown in Monnier et al. (2002) for WR140, but has since been used for Apep (Callingham et al., 2019; Han et al., 2020), WR104 (Harries et al., 2004), WR112 (Lau et al., 2020), WR137 (Lau et al., 2024), and WR140 (again, more accurately Han et al., 2022; Lau et al., 2022), with a high success when compared to CWB imagery.

Somewhat similar, independent models have been published since the creation of the aforementioned geo-

metric model. The first geometric treatment of the WCR alone was in Parkin & Pittard (2008), who modelled the shock region as a cone that rotated with orbital motion. This treatment of the geometric model involved implementing a 'skew' (a rotation of the WCR ring) to the WCR to account for the orbital motion of the secondary star. While this is apparently necessary to accurately model non-thermal emission from CWBs, it is not clear if this has significant effect on dust production that would manifest in imagery. An independent attempt at modelling the entire volumetric structure of the dust nebula was published in Williams et al. (2009) for WR140, where the results eccentric structure is close to that of Monnier et al. (2002), but with added effects of dust asymmetry not unlike Han et al. (2022).

These simpler geometric models offer significant computational efficiency at a cost of physical insight. Where a hydrodynamical simulation may take hours, days, or more, the geometric model can be evaluated on the order of seconds. This opens the door for parameter estimation using the geometric model rather than using it purely as a consistency check. As mentioned earlier, this does come at a cost of physical insight; with these geometric models we do not receive detailed information of dust production (e.g. dust mass, non-thermal emission, etc), but they do offer immediate information on more fundamental parameters such as orbital characteristics and dust turn on/off. As of yet, geometric models have not been used to constrain orbital parameters (eccentricity, inclination, etc) effectively, and a proper statistical treatment with Bayesian parameter inference methods has not been proven in the literature. Han et al. (2020) described their attempt at using Markov Chain Monte Carlo (MCMC) to infer binary parameters from the ridges of the geometric dust plume (rather than the entire image as a whole). They ultimately admitted failures in optimization as a result of the high dimensionality of the problem together with difficulty in creating an appropriate loss function that accounts for the complex ridge geometry in the nebula images. With direct imaging of CWB nebulae now occurring so regularly, using modern statistical methods to infer system parameters with these images is a key gap in the literature.

2 Progress Report

2.1 Introduction

A geometric model has emerged as a robust and fast method to reproduce observed colliding wind nebulae. The majority of orbital and wind parameters within colliding wind binaries are uniquely mapped by the corresponding parameters in the model, and so these models offer a modern and cheap way of understanding the underlying physics in these curious stellar systems. In this honours project we set out to develop a fast new implementation of the geometric model to study the Apep system, gaining insight into any unique effects and wind anisotropy. With this model, we aim to infer system parameters using modern statistical methods and obtain numerical parameter uncertainties for the first time. New data on Apep (and other notable CWB systems) is available and upcoming, including JWST MIRI observations and more VLT images, and so developing a model compatible with inference methods is more needed than ever before.

So far, no successful demonstration of Bayesian inference with this model has been published in the literature. With this in mind, from the ground up we have developed the fastest implementation of this geometric model with the Python framework JAX (Bradbury et al., 2018). JAX allows us to significantly speed up Python code written from scratch, and with this we have developed a geometric model which is 2 orders of magnitude faster per model evaluation than the previous implementation, at ~ 0.05 seconds. If a parameter sampling method like MCMC is the goal, several thousand model evaluations (at minimum) will need to be performed and a performant model is strictly necessary as a result. Further, these geometric models require over a dozen parameters

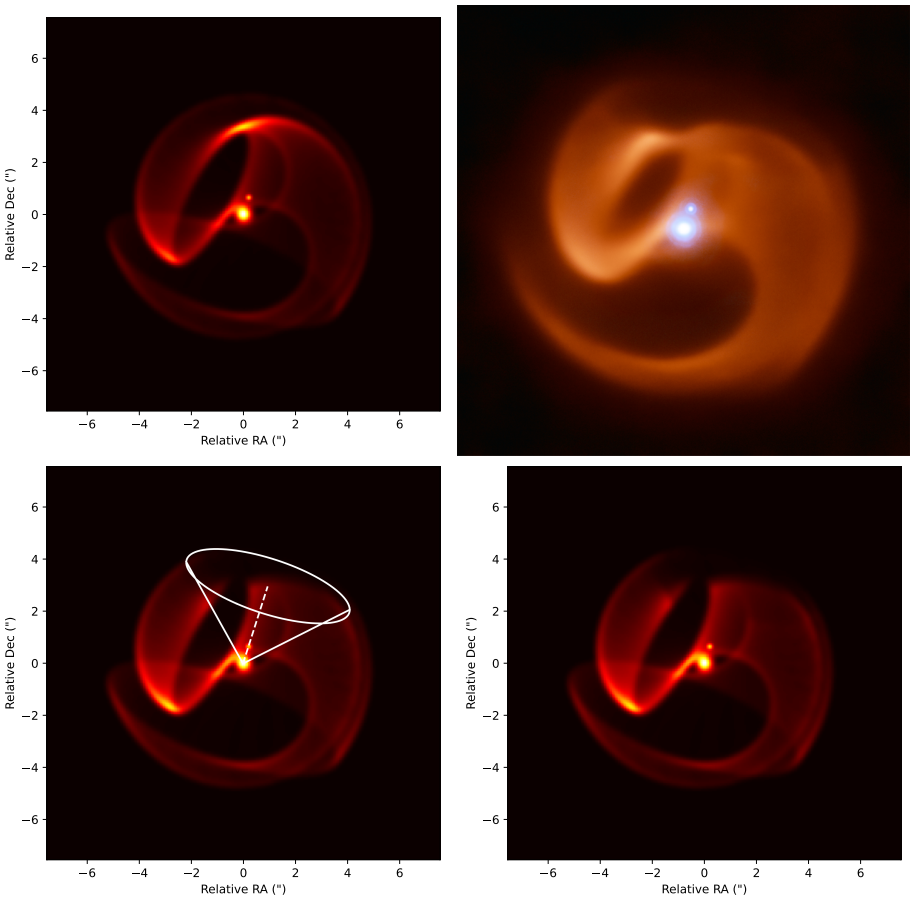

Figure. 4 We show the observational indication of photodissociation in the plume of Apep along the volume of a cone extending from the tertiary companion away from the inner binary. *Top left:* The geometric model of Apep without accounting for ternary plume effects. *Top right:* The ESO image of Apep in the near to mid infrared, clearly showing a cavity in the dust plume to the north north east. Image credit: ESO, Joseph Callingham. *Bottom left:* Our estimated cone parameters that best describe the top right image, 'destroying' the dust according to the Gaussian function in equation 7. Note in particular that the cone projection axis (dashed line) matches up with the position of the tertiary star by construction. *Bottom right:* The final model plume for Apep, taking into account these effects.

in their construction (and over two dozen when including extension physical effects like azimuthal/orbital variation), meaning that gradient-based Bayesian methods are needed. Fortunately, JAX is designed around automatic differentiation; any carefully written JAX function is able to have its gradient calculated with a comparable evaluation time to the base model. Our JAX-built geometric model is differentiable as a result, and, in principle, Hamiltonian Monte Carlo (HMC) is possible.

This fast and differentiable geometric model was designed to constrain the parameters of the Apep system in particular. As the Galaxy's foremost LGRB candidate, the somewhat uncertain orbital and stellar parameters of the system need to be more tightly constrained so that Apep's candidate LGRB status can be better understood and ideally confirmed or rejected. Such precision isn't possible without a detailed statistical analysis with Bayesian methods, and in doing so we aim to shed light on the possibility of LGRBs in the evolved Universe.

As a secondary objective with our custom made geometric model, we aim to definitively show whether or not the northern star in the Apep system is actually associated with the WR+WR binary. Ternary effects on a colliding wind nebula have never been modelled, and the physics involved is ripe for exploration. By showing a perturbation in the 'ideal' nebula (pertaining to just a binary system) is necessary to accurately model the Apep system, we may investigate how a third star can affect the evolution of these systems and their observables.

2.2 Creating a Geometric Model

The basic idea that underpins the geometric model is to approximate instantaneous dust production within the wind collision region as a ring. This ring is initialised in the orbital plane at the location of the 'secondary' star (in terms of wind strength, not mass as is convention), and ejected along the line of sight from the primary star to the secondary at the wind speed of the primary. As the two stars orbit each other, the direction of this ring ejection changes and the result is the 'wrapping' of the plume that creates the characteristic spiral.

Even at this basic level, the model has a multitude of parameters that can be changed at run time. The parameters most fundamental to this geometric approximation are the number of discretized points within each ring, and the number of rings to produce over the course of one orbital period. Ideally both of these would be as large as possible in order to reduce the error associated with approximating a continuous process as discrete (so called quantization error); practically we usually set these to be 400 points per ring and 1000 rings per orbit which provides a dense point cloud for the nebula.

To render the point cloud into an image that resembles the real nebulae, we can take a histogram of the line of sight projection of the cloud. Even though the point cloud extends into three dimensions, the projection of the real nebulae on the plane of the sky is effectively in two dimensions, and so by collapsing the 3D point cloud to a 2D image we can reproduce the observed images. By utilising the weighting functionality of histograms, we can selectively reduce the impact of points in order to emulate physical phenomena (e.g. dust turn off, azimuthal variation, etc).

In this section we describe the details of constructing this geometric model from scratch in JAX, and the additional features we have added to the model.

2.2.1 Ring Blowing

As previously mentioned, we generate a fixed number of rings per orbit. If the colliding wind binary episodically produces dust (e.g. WR 140, Apep, etc), the rings that are outside of the turn on/off true anomaly bounds have a weight of 0 in the histogram step. These rings are created at fixed time intervals throughout the orbits of the stars. This means that, for very eccentric systems which produce dust only close to periastron, fewer rings make up the dust plume compared to a constantly dust producing system as the stars spend less time near periastron than apastron. We would expect that the quantisation error would be correspondingly more prevalent in these systems, and hence we should produce more rings when attempting to fit systems such as WR 140.

We plan on implementing ring generation between only dust turn on and off (as opposed to across the entire orbit), and seeing how this compares with the existing implementation. This is non-trivial compared to the original Kepler problem due to the non-linearity in ring generation triggers in true anomaly (where it is linear in time).

Before rings can be created, we first need a model of the binary orbit so that we know where to initialise the rings and in what direction they move in. To calculate the true anomaly of a star at any point over the orbital period (i.e. with known mean anomaly, M), Kepler's equation

$$M = E - e \sin E \tag{1}$$

must be solved for the eccentric anomaly, E. From the eccentric anomaly, we can then calculate the true anomaly, ν, via

$$\nu = 2 \operatorname{atan2}\left(\sqrt{1+e}\sin(E/2),\ \sqrt{1-e}\cos(E/2)\right) \tag{2}$$

To solve Kepler's equation, we use the non-iterative method described in Markley (1995) and implemented in JAX in Hattori et al. (2024).

When the true anomaly at the current orbital position falls between that of the turn on and off threshold values, the produced rings contribute to the visible dust plume. We shouldn't expect, however, that the turn on or off of dust production is instantaneous, but rather that there is a gradual change in the production rate. Hence as an additional feature, we have implemented a turn on/off

smoothing in the dust production that was not present in previous versions of the geometric model. To do this, we use a Gaussian function to selectively increase the weight of rings that are outside of the usual dust production regime. That is, provided that $\nu_{\text{t\_off}} \leq \nu_{\text{ring}} \leq \nu_{\text{t\_on}}$ (i.e. the binary is not producing significant dust), we increase the weighting of a ring by

$$\Delta w = \exp\left(\frac{(\nu_{\text{ring}} - \nu_{\text{t\_on/offf}})^2}{2\sigma^2_{t\_on/off}}\right) \tag{3}$$

where we calculate this twice, once for each of gradual turn on at $\nu_{\text{t\_on}}$ and gradual turn off at $\nu_{\text{t\_off}}$, and the rate of turn on/off is decided by the standard deviation $\sigma_{t\_on/off}$ in units of true anomaly.

2.2.2 Azimuthal and Orbital Variation in Dust Production

As part of the model, we implement the optional azimuthal and orbital variation of dust production described in Han et al. (2022). Like in their paper, we model these variations as Gaussian function multipliers applied to each particle within a ring and each entire ring respectively. The azimuthal variation in dust production is modelled as

$$\delta w = (1 - A_{\text{az}})\ \exp\left(-\frac{(\theta_{\text{particle}} - \theta_{\text{az\_min}})^2}{2\sigma^2_{\text{az}}}\right) \tag{4}$$

which is multiplied across the weights of all of the particles in a ring, and where A_{az} is the strength of the variation, $\theta_{\text{particles}}$ is the angular coordinate of each particle within a ring, $\theta_{\text{az\_min}}$ is the location of the azimuthal minimumm and σ_{az} is the spread of the variation across the angular coordinates of the particles. Although each of these parameters can be custom chosen, we usually set $\theta_{\text{az\_min}} = 90°$ in practice, corresponding to the leading edge of the dust plume with respect to the orbital motion (that is, dust production is weaker at the leading edge).

Similarly, the orbital variation in dust production is also modelled as a Gaussian multiplier,

$$\delta w = (1 - A_{\text{orb}})\ \exp\left(-\frac{(\nu_{\text{ring}} - \nu_{\text{orb\_min}})^2}{2\sigma^2_{\text{orb}}}\right) \tag{5}$$

which is applied to an entire rings weighting. The parameters in this Gaussian are analogous to that of the azimuthal variation, instead using the true anomaly of the ring instead of a particle angular coordinate, and with orbital variation amplitudes and spreads instead of azimuthal. We usually set $\nu_{\text{orb, min}} = 180°$, corresponding to the periastron of the orbit where the dust production may be weak during the dust production phase.

2.2.3 Photodissociation from a Tertiary Star

Early on in the project, we noticed that the previous best model of Apep (top left in Figure 4) misses a lot of the geometry in the plume. Upon realising that the cavity in the plume aligned perfectly with the apparent position of the Northern companion of Apep's inner binary, we began investigating how a far off third companion could influence a colliding wind nebula. The most dominant effect appears to be photodissociation of the already formed dust once it collides with the tertiary O star wind. With this in mind, in our model we 'destroy' dust that falls within some angular distance of the tertiary star with respect to the inner WR+WR binary.

Like the generation of the colliding wind nebula, the photodissociation region predominately relies on a few key parameters: the position of the tertiary star with respect to the inner binary and the cone open angle of the region. For the former, in the code we define the position of the third star in spherical coordinates with respect to the inner binary orbital plane. That is, we choose the angular location of the photodissociation region with a polar and azimuthal angle, and the radial location of the third star with a distance parameter. The photodissociation cone open angle is chosen to best fit the observed nebula by eye, and we aim to constrain this with numerical methods later on in the project.

With the parameters chosen, we affect the weight of generated points whose angular distance is close enough to the center of the cone projection axis. To calculate the angular distance, we use the formula from (Kells & Kern, 1940), modified to fit with the convention that the inclination $\theta = 0$ is at the north pole rather than $\theta = -\pi/2$:

$$\begin{aligned}\alpha = \arccos\big[&\cos(\theta_{\text{comp}})\cos(\theta_{\text{part}}) + \\ &+ \sin(\theta_{\text{comp}})\sin(\theta_{\text{part}})\cos(\phi_{\text{comp}} - \phi_{\text{part}})\big]\end{aligned} \tag{6}$$

At present, we do not necessarily set all of these point weights to 0 but rather de-weight them by a Gaussian according to how far each point is from the cones central angular coordinate:

$$\Delta w = -A_{\text{comp}} \exp\left(-\frac{2(\Delta\theta)^2}{\theta^2_{\text{OA,comp}}}\right) \tag{7}$$

where A_{comp} is the amplitude of the photodissociation, $\Delta\theta$ is the angular distance for each particle from the center of the cone, and $\theta_{\text{OA,comp}}$ is the photodissociation region open angle.

Figure 4 shows the effect of this feature in relation to the observed Apep image. We think that the geometry, while still not a perfect fit to the true image, is a notable step in the right direction in understanding Apep's unique nebula. Tertiary effects in WR CWBs have been observed before (notably in WR 147), although no evidence of photodissociation as a result of this has been shown in the literature.

Perhaps the last – or one of the last – mysteries in Apep's colliding wind nebula is the origin of the horizontal ridge outlining the cavity just above the tertiary

star in the image. We plan to investigate this further, and posit that it may be the result of the tertiary star partially blowing the dust away rather than completely destroying it.

2.3 Inference with the Geometric Model

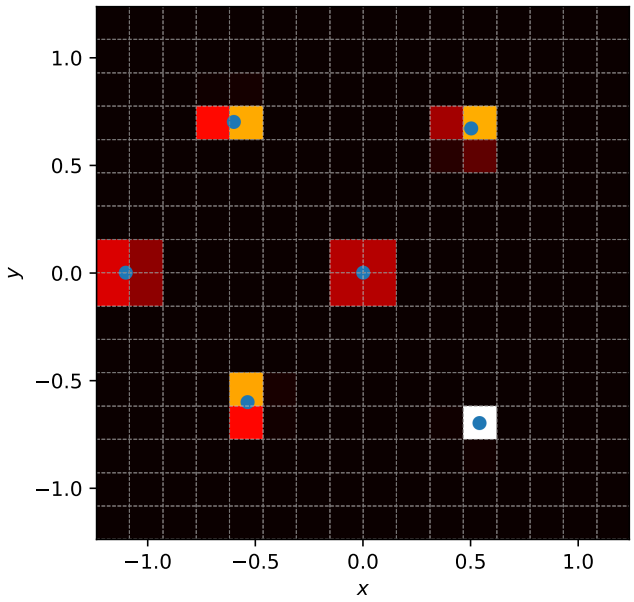

Figure. 5 We show the behaviour of the smooth histogram at all key criteria. The true positions of points are shown as a blue dot, and the associated smooth histogram representation is shown in the bins (here with a grid size of $N = 16$). Dot positions were manually chosen so that all behaviours are shown in the same plot. Brighter values of the colourmap represent larger bin values.

Although JAX allows us to automatically calculate gradients of our model, these gradients are not always reliable. The reason for this is not a flaw in the JAX pipeline but in the programming of our model and renderer: a computer does exactly what we tell it to.

Perhaps the most obvious problem in the calculated gradients of our geometric model pipeline is in the renderer; after generating the three dimensional point cloud, we take a histogram of the points to generate an image. Histograms are, however, not smoothly differentiable due to their inherent discrete representation of data. For example, a point in one dimension may be in the center of a histogram bin, or it may be on the extreme edge of the bin, and the bin count increases by one all the same. One can imagine moving this point smoothly in one dimension (e.g. from the center of a bin to the edge of the same bin) and even though the absolute coordinate of the point has changed, the bin count remains steady. Suddenly, as the point moves from the edge of one bin to another, there is a discontinuous drop in the count of the first bin and conversely a discontinuous increase in the count of the other. Discontinuities are problematic for gradients, and so a gradient friendly renderer is needed.

Our devised solution acts fundamentally as a histogramming tool still, but by spreading density information of each point to all of the neighbouring bins of a point. We show the behaviour of our 'smooth histogram' renderer in Figure 5 in two dimensions (applicable for our rendering). The 'count' of each neighbouring bin of a point is chosen based on the area overlap of a square (with side length of the bin size) centered on the point exactly. The bin that the point is in will have the most area overlap of this square and so will have the highest 'count' (appear brighter in the figure). If a point is left of center of a bin, the neighbouring left bin will have some 'count' added to it, and analogously for the top, down, and left directions.

The equations to calculate the contribution to each bin are made easier with a change of coordinates. If a point at position (x, y) is α away from the closest left-/right edge of its resident bin and β away from the top/-down edge of its bin (i.e. $\alpha = x \mod L$ and $\beta = y \mod L$ for L bin side length), we can define new coordinates

$$a = \min\{\alpha,\, L - \alpha\} + L/2 \tag{8}$$
$$b = \min\{\beta,\, L - \beta\} + L/2 \tag{9}$$

where the $+L/2$ for each dimension arises from the fact that the overlapping square is centered on the point absolute coordinate. With these, the contributions to each of the main (that the point lies in), horizontal neighbouring, vertical neighbouring, and diagonal neighbouring bins are

$$A_{\text{main}} = ab \tag{10}$$
$$A_{\text{horiz}} = (L - a)\, b \tag{11}$$
$$A_{\text{vert}} = a\,(L - b) \tag{12}$$
$$A_{\text{diag}} = (L - a)(L - b) \tag{13}$$

We can see in Figure 5 that when a point is directly in the center of a bin, this just reduces to normal histogramming behaviour where only one bin total is changed. When a point is directly centered on one axis (vertical or horizontal), only the other axis gets a count contribution spread to neighbouring bins. When a point is directly on the corner of a bin, all neighbouring bins get the same count contribution. As a point moves, the contributions to each neighbouring bin change smoothly, and therefore so does the gradient. This allows us to remain working with a relatively simple renderer for our plume point cloud, while preserving the gradients of our plume model.

2.4 Future Work

In the first 6 months of the project, we have developed a geometric model with gradients that is $\sim$ 100 times

faster than the previous implementation, shown ternary effects in Apep, developed a GUI interface for the model and more, but there is still much work to be done.

While automatic differentiation with JAX allows us to calculate gradients of our model, these gradients are currently too unstable for inference methods. Fundamental choices made within the model, e.g. the number of points in each ring, the number of rings per orbit, where these rings are initialised, etc, all affect the numerical stability of the gradients. We are actively investigating sources of instability in the gradients, and these need to be fixed before HMC with our model is realistic.

In terms of science with Apep, there are still questions to be answered. There may be anisotropic winds in the main dust producer of Apep as suggested in Callingham et al. (2019), but the effect of this on the visible dust plume are not clear. We aim to implement an anisotropic wind model together with a spin-orbit misalignment of the primary WR star in Apep to investigate how these differing windspeeds affect the plume geometry. There are models of anisotropic winds in the literature (Poe et al., 1989; Bloot et al., 2022, e.g.) with which we can begin from in our analysis. These models often require certain physical properties at the surface of stars; in particular a weak magnetic field is required so that the star can maintain enough angular momentum for an anisotropic wind, however Wolf-Rayet magnetic fields are not well understood and may be strong or weak (Hubrig et al., 2020; Bloot et al., 2022).

Apep is due to be observed with JWST within the next 2 months, giving us another dataset within the honours project to analyse. From recent JWST observations of WR140, we expect that at least one or more shells will be resolved with the telescope compared to the VLT observations (Figure 2; Lau et al., 2022). Since Apep has an orbital period of ~ 100 years, this will allow us to monitor the long term behaviour of the system and possibly see a variation in the cavity position from the orbital motion of the third star. In addition to this, there is a JWST MIRI observing program imaging four other CWBs over the next few months: WR48a, WR112, WR125, and WR137. Time permitting, we hope to be able to fit geometric models to these systems at the very least, and optimistically we may be able to use HMC to infer system parameters.

In addition to these new JWST datasets, the VLT recently imaged Apep once more. This 2024 epoch, in addition to the previous 2016/17/18 epochs will allow us to strongly constrain the expansion speed of the Apep nebula and hence the windspeed of the primary. As well as this, we have access to 2023 and 2024 epochs of VLTI data on the inner binary of Apep – resolving the two WR stars – and have been granted an additional epoch in 2025. With these three epochs, we aim to constrain the possible orbits of the WR+WR inner binary in conjunction with the observed plume.

Finally, Han et al. (2022) showed that there is a strong indication of radiative acceleration in the dust plume of WR140. Their method showing this was not in the actual geometric model itself, however, and we aim to implement this dust acceleration within our geometric model to more accurately model WR140's plume and investigate whether acceleration is evident in other CWB plumes.

References

Abbott D. C., Conti P. S., 1987, ARA&A, 25, 113

Aguilera-Dena D. R., Langer N., Moriya T. J., Schootemeijer A., 2018, ApJ, 858, 115

Allen D. A., Swings J. P., Harvey P. M., 1972, A&A, 20, 333

Ashall C., et al., 2019, MNRAS, 487, 5824

Barlow M. J., Smith L. J., Willis A. J., 1981, MNRAS, 196, 101

Baug T., de Grijs R., Dewangan L. K., Herczeg G. J., Ojha D. K., Wang K., Deng L., Bhatt B. C., 2019, ApJ, 885, 68

Bavera S. S., et al., 2022, A&A, 657, L8

Berger E., 2014, ARA&A, 52, 43

Bloot S., Callingham J. R., Marcote B., 2022, MNRAS, 509, 475

Bonanos A. Z., et al., 2004, ApJ, 611, L33

Bradbury J., et al., 2018, JAX: composable transformations of Python+NumPy programs, `http://github.com/google/jax`

Callingham J. R., Tuthill P. G., Pope B. J. S., Williams P. M., Crowther P. A., Edwards M., Norris B., Kedziora-Chudczer L., 2019, Nature Astronomy, 3, 82

Callingham J. R., Crowther P. A., Williams P. M., Tuthill P. G., Han Y., Pope B. J. S., Marcote B., 2020, MNRAS, 495, 3323

Carroll B. W., Ostlie D. A., 2017, An Introduction to Modern Astrophysics, Second Edition. Cambridge University Press

Castor J. I., Abbott D. C., Klein R. I., 1975, ApJ, 195, 157

Chené A.-N., St-Louis N., Moffat A. F. J., Gayley K. G., 2020, ApJ, 903, 113

Cherchneff I., Le Teuff Y. H., Williams P. M., Tielens A. G. G. M., 2000, A&A, 357, 572

Cherepashchuk A. M., 1976, Soviet Astronomy Letters, 2, 138

Chiappini C., Hirschi R., Meynet G., Ekström S., Maeder A., Matteucci F., 2006, A&A, 449, L27

Chira R. A., Kainulainen J., Ibáñez-Mejía J. C., Henning T., Mac Low M. M., 2018, A&A, 610, A62

Chrimes A. A., Stanway E. R., Eldridge J. J., 2020, MNRAS, 491, 3479

Cichowolski S., Suad L. A., Pineault S., Noriega-Crespo A., Arnal E. M., Flagey N., 2015, MNRAS, 450, 3458

Conti P. S., 1975, Memoires of the Societe Royale des Sciences de Liege, 9, 193

Crowther P. A., 2007, ARA&A, 45, 177

Dale J. E., Ngoumou J., Ercolano B., Bonnell I. A., 2013, MNRAS, 436, 3430

De Becker M., Raucq F., 2013, A&A, 558, A28

De Marco O., Izzard R. G., 2017, PASA, 34, e001

Dean C., Fernández R., 2024, Phys. Rev. D, 109, 083010

Detmers R. G., Langer N., Podsiadlowski P., Izzard R. G., 2008, A&A, 484, 831
Dougherty S. M., Beasley A. J., Claussen M. J., Zauderer B. A., Bolingbroke N. J., 2005, ApJ, 623, 447
Dsilva K., Shenar T., Sana H., Marchant P., 2020, A&A, 641, A26
Dsilva K., Shenar T., Sana H., Marchant P., 2022, A&A, 664, A93
Dsilva K., Shenar T., Sana H., Marchant P., 2023, A&A, 674, A88
Eatson J. W., Pittard J. M., Van Loo S., 2022a, MNRAS, 516, 6132
Eatson J. W., Pittard J. M., Van Loo S., 2022b, MNRAS, 517, 4705
Eichler D., Usov V., 1993, ApJ, 402, 271
Eldridge J. J., Langer N., Tout C. A., 2011, MNRAS, 414, 3501
Eldridge J. J., Fraser M., Smartt S. J., Maund J. R., Crockett R. M., 2013, MNRAS, 436, 774
Filippenko A. V., 1997, ARA&A, 35, 309
Foellmi C., Moffat A. F. J., Guerrero M. A., 2003, MNRAS, 338, 1025
Galama T. J., et al., 1998, Nature, 395, 670
Gamow G., 1943, ApJ, 98, 500
Gehrz R. D., Hackwell J. A., 1974, ApJ, 194, 619
Gosset E., Nazé Y., 2016, A&A, 590, A113
Gräfener G., Hamann W. R., 2008, A&A, 482, 945
Gräfener G., Vink J. S., de Koter A., Langer N., 2011, A&A, 535, A56
Groh J. H., Meynet G., Georgy C., Ekström S., 2013, A&A, 558, A131
Hacar A., Clark S. E., Heitsch F., Kainulainen J., Panopoulou G. V., Seifried D., Smith R., 2023, in Inutsuka S., Aikawa Y., Muto T., Tomida K., Tamura M., eds, Astronomical Society of the Pacific Conference Series Vol. 534, Protostars and Planets VII. p. 153 (arXiv:2203.09562), doi:10.48550/arXiv.2203.09562
Hamann W. R., Gräfener G., Liermann A., 2006, A&A, 457, 1015
Han Y., et al., 2020, MNRAS, 498, 5604
Han Y., Tuthill P. G., Lau R. M., Soulain A., 2022, Nature, 610, 269
Harries T. J., Babler B. L., Fox G. K., 2000, A&A, 361, 273
Harries T. J., Monnier J. D., Symington N. H., Kurosawa R., 2004, MNRAS, 350, 565
Hattori S., Garcia L., Murray C., Dong J., Dholakia S., Degen D., Foreman-Mackey D., 2024, exoplanet-dev/jaxoplanet: Astronomical time series analysis with JAX, doi:10.5281/zenodo.10736936, https://doi.org/10.5281/zenodo.10736936
Hendrix T., Keppens R., van Marle A. J., Camps P., Baes M., Meliani Z., 2016, MNRAS, 460, 3975
Hoyle F., 1953, ApJ, 118, 513
Hubrig S., Schöller M., Cikota A., Järvinen S. P., 2020, MNRAS, 499, L116
Hurtado V. U., Lloyd-Ronning N. M., Miller J. M., 2024, ApJ, 967, L4
Josiek J., Ekström S., Sander A. A. C., 2024, arXiv e-prints, p. arXiv:2404.14488
Karamehmetoglu E., et al., 2023, A&A, 678, A87
Kells L. M., Kern W. F., 1940, Plane and Spherical Trigonometry, 2nd ed. edn. McGraw Hill Book Company, New York
Kilpatrick C. D., et al., 2021, MNRAS, 504, 2073
Kroupa P., 2001, MNRAS, 322, 231
Lamberts A., Dubus G., Lesur G., Fromang S., 2012, A&A, 546, A60
Lau R. M., Hankins M. J., Schödel R., Sanchez-Bermudez J., Moffat A. F. J., Ressler M. E., 2017, ApJ, 835, L31
Lau R. M., et al., 2020, ApJ, 900, 190
Lau R. M., et al., 2021, ApJ, 909, 113
Lau R. M., et al., 2022, Nature Astronomy, 6, 1308
Lau R. M., et al., 2023, ApJ, 951, 89
Lau R. M., et al., 2024, ApJ, 963, 127
Lefèvre L., et al., 2005, MNRAS, 360, 141
Mackey J., Jones T. A. K., Brose R., Grassitelli L., Reville B., Mathew A., 2023, MNRAS, 526, 3099
Maeder A., 1983, A&A, 120, 113
Marchenko S. V., Moffat A. F. J., 2007, in St. -Louis N., Moffat A. F. J., eds, Astronomical Society of the Pacific Conference Series Vol. 367, Massive Stars in Interactive Binaries. p. 213 (arXiv:astro-ph/0610531), doi:10.48550/arXiv.astro-ph/0610531
Marchenko S. V., Moffat A. F. J., Vacca W. D., Côté S., Doyon R., 2002, ApJ, 565, L59
Marchenko S. V., Moffat A. F. J., Crowther P. A., 2010, ApJ, 724, L90
Marcote B., Callingham J. R., De Becker M., Edwards P. G., Han Y., Schulz R., Stevens J., Tuthill P. G., 2021, MNRAS, 501, 2478
Markley F. L., 1995, Celestial Mechanics and Dynamical Astronomy, 63, 101
McClelland L. A. S., Eldridge J. J., 2016, MNRAS, 459, 1505
Meynet G., Georgy C., Hirschi R., Maeder A., Massey P., Przybilla N., Nieva M. F., 2011, Bulletin de la Societe Royale des Sciences de Liege, 80, 266
Michaux Y. J. L., Moffat A. F. J., Chené A.-N., St-Louis N., 2014, MNRAS, 440, 2
Miller G. E., Scalo J. M., 1979, ApJS, 41, 513
Monnier J. D., Tuthill P. G., Danchi W. C., 1999, ApJ, 525, L97
Monnier J. D., Tuthill P. G., Danchi W. C., 2002, ApJ, 567, L137
Monnier J. D., et al., 2011, ApJ, 742, L1
Motte F., Bontemps S., Louvet F., 2018, ARA&A, 56, 41
Offner S. S. R., Moe M., Kratter K. M., Sadavoy S. I., Jensen E. L. N., Tobin J. J., 2023, in Inutsuka S., Aikawa Y., Muto T., Tomida K., Tamura M., eds, Astronomical Society of the Pacific Conference Series Vol. 534, Protostars and Planets VII. p. 275 (arXiv:2203.10066), doi:10.48550/arXiv.2203.10066
Paczyński B., 1967, Acta Astron., 17, 355
Parkin E. R., Pittard J. M., 2008, MNRAS, 388, 1047
Peatt M. J., Richardson N. D., Williams P. M., Karnath N., Shenavrin V. I., Lau R. M., Moffat A. F. J., Weigelt G., 2023, ApJ, 956, 109
Pellegrino C., et al., 2022, ApJ, 938, 73
Pittard J. M., Dougherty S. M., 2006, MNRAS, 372, 801
Pledger J. L., Sharp A. J., Sansom A. E., 2021, MNRAS, 503,

2168
Poe C. H., Friend D. B., Cassinelli J. P., 1989, ApJ, 337, 888
Prilutskii O. F., Usov V. V., 1976, Soviet Ast., 20, 2
Rauw G., Nazé Y., 2016, Advances in Space Research, 58, 761
Rauw G., et al., 2005, A&A, 432, 985
Richardson N. D., et al., 2024, arXiv e-prints, p. arXiv:2405.10454
Rodríguez L. F., Arthur J., Montes G., Carrasco-González C., Toalá J. A., 2020, ApJ, 900, L3
Salpeter E. E., 1952, ApJ, 115, 326
Sana H., 2017, in Eldridge J. J., Bray J. C., McClelland L. A. S., Xiao L., eds, Vol. 329, The Lives and Death-Throes of Massive Stars. pp 110–117 (arXiv:1703.01608), doi:10.1017/S1743921317003209
Sana H., Evans C. J., 2011, in Neiner C., Wade G., Meynet G., Peters G., eds, Vol. 272, Active OB Stars: Structure, Evolution, Mass Loss, and Critical Limits. pp 474–485 (arXiv:1009.4197), doi:10.1017/S1743921311011124
Sander A. A. C., Vink J. S., 2020, MNRAS, 499, 873
Schönberner D., Balick B., Jacob R., 2018, A&A, 609, A126
Schootemeijer A., Shenar T., Langer N., Grin N., Sana H., Schürmann G. G. C., Wang C., Xu X. T., 2024, arXiv e-prints, p. arXiv:2406.01420
Seaquist E. R., 1976, ApJ, 203, L35
Shara M. M., Howell S. B., Furlan E., Gnilka C. L., Moffat A. F. J., Scott N. J., Zurek D., 2022, MNRAS, 509, 2897
Shenar T., Hamann W. R., Todt H., 2014, A&A, 562, A118
Shenar T., et al., 2017, A&A, 598, A85
Shenar T., Gilkis A., Vink J. S., Sana H., Sander A. A. C., 2020, A&A, 634, A79
Siebert M. R., et al., 2024, arXiv e-prints, p. arXiv:2406.05076
Smartt S. J., 2009, ARA&A, 47, 63
Soulain A., et al., 2018, A&A, 618, A108
Soulain A., Lamberts A., Millour F., Tuthill P., Lau R. M., 2023, MNRAS, 518, 3211
Tan J. C., Beltrán M. T., Caselli P., Fontani F., Fuente A., Krumholz M. R., McKee C. F., Stolte A., 2014, in Beuther H., Klessen R. S., Dullemond C. P., Henning T., eds, Protostars and Planets VI. pp 149–172 (arXiv:1402.0919), doi:10.2458/azu˙uapress˙9780816531240-ch007
Tolstoy E., Hill V., Tosi M., 2009, ARA&A, 47, 371
Tuthill P. G., Monnier J. D., Danchi W. C., 1999, Nature, 398, 487
Tuthill P., Monnier J., Tanner A., Figer D., Ghez A., Danchi W., 2006, Science, 313, 935
Tuthill P. G., Monnier J. D., Lawrance N., Danchi W. C., Owocki S. P., Gayley K. G., 2008, ApJ, 675, 698
Ud-Doula A., Owocki S. P., Townsend R. H. D., 2009, MNRAS, 392, 1022
Usov V. V., 1991, MNRAS, 252, 49
Vink J. S., Harries T. J., 2017, A&A, 603, A120
Vink J. S., de Koter A., 2005, A&A, 442, 587
Vink J. S., Gräfener G., Harries T. J., 2011, A&A, 536, L10
Vrancken M., De Greve J. P., Yungelson L., Tutukov A., 1991, A&A, 249, 411
Wallace D. J., Moffat A. F. J., Shara M. M., 2002, in Moffat A. F. J., St-Louis N., eds, Astronomical Society of the Pacific Conference Series Vol. 260, Interacting Winds from Massive Stars. p. 407
Williams P. M., 2019, MNRAS, 488, 1282
Williams P. M., Beattie D. H., Lee T. J., Stewart J. M., Antonopoulou E., 1978, MNRAS, 185, 467
Williams P. M., van der Hucht K. A., The P. S., 1987, QJRAS, 28, 248
Williams P. M., van der Hucht K. A., Pollock A. M. T., Florkowski D. R., van der Woerd H., Wamsteker W. M., 1990, MNRAS, 243, 662
Williams P. M., et al., 2009, MNRAS, 395, 1749
Williams P. M., van der Hucht K. A., van Wyk F., Marang F., Whitelock P. A., Bouchet P., Setia Gunawan D. Y. A., 2012, MNRAS, 420, 2526
Williams P. M., et al., 2021, MNRAS, 503, 643
Willis A. J., 1982, MNRAS, 198, 897
Wolf C. J. E., Rayet G., 1867, Academie des Sciences Paris Comptes Rendus, 65, 292
Woosley S. E., 1993, ApJ, 405, 273
Woosley S. E., Bloom J. S., 2006, ARA&A, 44, 507
Woosley S. E., Heger A., 2006, ApJ, 637, 914
Woosley S. E., Heger A., Weaver T. A., 2002, Reviews of Modern Physics, 74, 1015
Zavala S., Toalá J. A., Santamaría E., Ramos-Larios G., Sabin L., Quino-Mendoza J. A., Rubio G., Guerrero M. A., 2022, MNRAS, 513, 3317
Zhekov S. A., 2021, MNRAS, 500, 4837
Zhekov S. A., Park S., 2010a, ApJ, 709, L119
Zhekov S. A., Park S., 2010b, ApJ, 721, 518
Zhekov S. A., Tomov T., Gawronski M. P., Georgiev L. N., Borissova J., Kurtev R., Gagné M., Hajduk M., 2014, MNRAS, 445, 1663
Zhekov S. A., Gagné M., Skinner S. L., 2022, MNRAS, 510, 1278
de Wit W. J., Testi L., Palla F., Zinnecker H., 2005, A&A, 437, 247
van der Hucht K. A., 2001, New A Rev., 45, 135
van der Hucht K. A., et al., 1996, A&A, 315, L193